

NANOVESICLE TRAPPING FOR STUDYING WEAK PROTEIN INTERACTIONS BY SINGLE-MOLECULE FRET

Jaime J. Benítez, Aaron M. Keller, and Peng Chen

Contents

| | |
|---|----|
| 1. Introduction | 42 |
| 2. Nanovesicle Trapping Approach | 44 |
| 2.1. Lipid selection | 45 |
| 2.2. Lipid nanovesicle preparation and protein trapping | 46 |
| 3. smFRET Measurements of Weak Protein–Protein Interactions | 47 |
| 3.1. Surface immobilization of nanovesicles | 47 |
| 3.2. Control experiments | 49 |
| 3.3. Application to weak interactions between intracellular copper transporters | 51 |
| 4. Single-Molecule Kinetic Analysis of Three-State Protein–Protein Interactions | 54 |
| 5. Further Developments | 57 |
| 6. Concluding Remarks | 58 |
| Acknowledgments | 59 |
| References | 59 |

Abstract

Protein–protein interactions are fundamental biological processes. While strong protein interactions are amenable to many characterization techniques including crystallography, weak protein interactions are challenging to study because of their dynamic nature. Single-molecule fluorescence resonance energy transfer (smFRET) can monitor dynamic protein interactions in real time, but are generally limited to strong interacting pairs because of the low concentrations needed for single-molecule detection. Here, we describe a nanovesicle trapping approach to enable smFRET study of weak protein interactions at high effective concentrations. We describe the experimental procedures, summarize the application in studying the weak interactions between intracellular copper transporters, and detail the single-molecule kinetic analysis

Department of Chemistry and Chemical Biology, Cornell University, Ithaca, New York, USA

of bimolecular interactions involving three states. Both the experimental approach and the theoretical analysis are generally applicable to studying many other biological processes at the single-molecule level.

1. INTRODUCTION

Protein–protein interactions are essential for cellular functions including protein folding, cell signaling, and metal trafficking (Gragerov *et al.*, 1992; Hall, 1992; Huffman and O’Halloran, 2001). The strength of protein–protein interactions can vary widely depending on the proteins involved. Strong protein interactions can have equilibrium dissociation constants (K_D) of a few picomolar ($10^{-12}M$), for example antigen–antibody interactions, for which tight binding is crucial (Nooren and Thornton, 2003). Weak protein interactions can have K_D ’s of a few micromolar to millimolar (10^{-6} – $10^{-3}M$), for example, interactions between metallochaperones and their target proteins, for which dynamic binding and unbinding are necessary to have many interaction turnovers (Banci and Rosato, 2003; Cobine *et al.*, 2006; Huffman and O’Halloran, 2001; Kim *et al.*, 2008; Lutsenko *et al.*, 2007; Rosenzweig, 2001; Strausak *et al.*, 2003).

For understanding their fundamental properties, strong protein interactions are amenable to characterization by ensemble measurements, as stable interaction complexes can form even at dilute solution conditions. Stable protein complexes can further be crystallized for structural determination down to atomic resolution. In contrast, weak protein interactions are challenging to characterize in ensemble measurements for several reasons: (1) they are dynamic and stochastic, making synchronization of molecular actions often necessary; (2) the steady-state concentrations of interaction intermediates are often low, making detection difficult; and (3) the presence of multiple interaction intermediates can complicate ensemble-averaged measurements. To study these weak protein interactions, single-molecule measurements offer several advantages: (1) no synchronization of molecular reactions is necessary; (2) the molecular reactions, including the formation, interconversion, and dissolution of interaction intermediates, are followed in real time; and (3) only one molecular state, be it an intermediate, is observed at any time point, enabling the resolution of complex reaction kinetics.

Single-molecule fluorescence resonance energy transfer (smFRET), with its inherent distance dependence in the nanometer scale, is particularly suited for probing dynamic protein–protein interactions, which is accompanied by changes in protein–protein distances. There are challenges to overcome, however, before smFRET can be applied to study weak protein interactions. The primary challenge is the concentration limit. Single-molecule fluorescence measurements are generally done at low

concentrations ($< 10^{-9} M$) to spatially separate fluorophores so that there is less than one fluorophore (or one pair of fluorophores) on average in the detection volume (about 10^{-16} – 10^{-15} l) monitored in confocal microscopy or total internal reflection microscopy. This low concentration range limits single-molecule protein interaction studies to strong interacting pairs, whereas weak protein interactions need to be studied at much higher concentrations ($> 10^{-6} M$) to favor complex formation.

To overcome this concentration limit, one needs to decrease the effective detection volume to $\sim 10^{-19}$ – 10^{-21} l, so that at concentrations of up to 10^{-6} – $10^{-4} M$ there is no more than one fluorophore on average found in it (Laurence and Weiss, 2003). This can be done by reducing the laser excitation volume or by confining molecules in space.

For reducing the excitation volume, Webb, Craighead, and coworkers have fabricated zero-mode waveguides made of metal-clad wells on top of a silica substrate (Levene *et al.*, 2003). The diameter of these wells is much smaller than the wavelength of the excitation light, and therefore, light shining at the silica substrate cannot propagate through the wells. This blockage of light propagation reduces the light excitation to an evanescent electromagnetic field close to the silica substrate surface, leading to reduction of the laser excitation volume to $\sim 10^{-21}$ l. Using this approach, Webb, Craighead, and coworkers have studied the reactions of individual DNA polymerase molecules that have substrate binding affinity in the micromolar range. As these zero-mode waveguides are open reaction containers, a big advantage is easy exchange of solutions for changing reaction conditions. A disadvantage is the proximity of a metal surface to the fluorophore; the metal surface can influence the fluorophore's fluorescence properties, such as its intensity and fluorescence lifetime. To follow individual molecules over time, the molecules also have to be immobilized on the silica surface at the bottom of the wells, which can introduce nonspecific surface interactions.

For confining molecules spatially, trapping with nanometer-sized lipid vesicles is an effective approach (Fig. 4.1), which was initially used in single-molecule studies of enzyme reactions (Chiu *et al.*, 1999), protein folding (Boukobza *et al.*, 2001; Haran, 2003; Rhoades *et al.*, 2003, 2004), and nucleic acid conformation dynamics (Lee *et al.*, 2005; Okumus *et al.*, 2004). Because of the confined volume, the effective concentration of a single-molecule inside a nanovesicle can be as high as tens of micromolar, while the overall concentration of the nanovesicles can be kept low to maintain the single-molecule detection condition. Using this nanovesicle trapping approach combined with smFRET measurements, Ha and coworkers have studied dynamic protein–nucleic acid interactions (Cisse *et al.*, 2007), and we have studied weak protein–protein interactions at high effective concentrations (Benitez *et al.*, 2008, 2009). In this chapter, we describe in detail how nanovesicle trapping, combined with smFRET

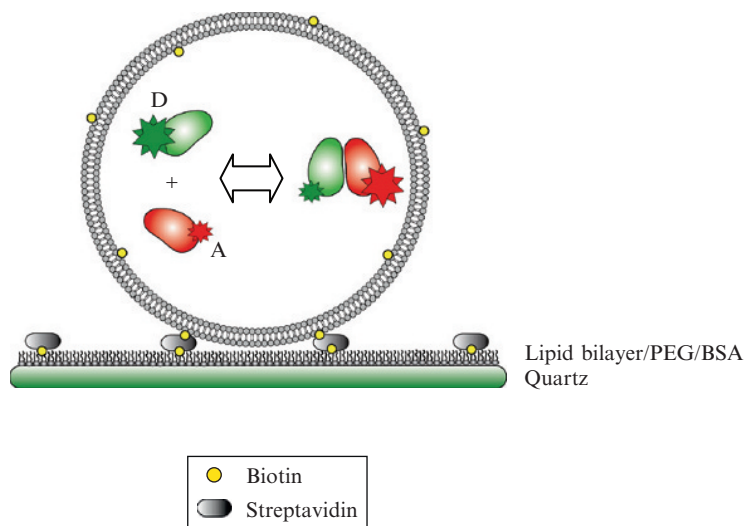


Figure 4.1 Schematics of nanovesicle trapping of two proteins labeled with a FRET donor–acceptor pair for smFRET studies.

measurements, can be used to characterize weak, dynamic protein interactions at the single-molecule level. We also detail the single-molecule kinetic analysis of bimolecular interactions that show three FRET states.

2. NANOVESICLE TRAPPING APPROACH

Nanovesicle trapping is an effective approach in reducing the effective detection volume to enable high concentration studies at the single-molecule level. This approach also offers several other advantages: (1) the lipid membrane enclosure mimics biological environments inside cells or organelles; (2) the membrane prevents nonspecific interactions between the protein and the glass surface because molecule immobilization is done via tethering the nanovesicle (Fig. 4.1); nevertheless, nonspecific interactions with the lipid membrane may occur; control experiments must be performed to check this possibility (see below); (3) the diameter of vesicles can be varied from a few hundred nanometers down to ~ 50 nm, covering effective concentrations of up to $\sim 24 \mu\text{M}$ for a single-molecule inside (Fig. 4.2); and (4) for protein–protein interaction studies, interactions between molecules of the same type, if occurring, can be selectively discarded in the data analysis stage by examining only the nanovesicles that contain molecules of different types.

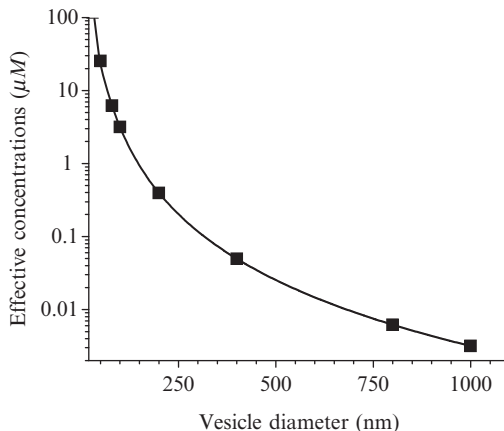


Figure 4.2 Dependence of the effective concentration of a single molecule on the diameter of the nanovesicle. The solid symbols indicate a few commercial available membrane pore sizes for preparing nanovesicles.

In this section, we describe the experimental details of preparing nanovesicles to trap two different proteins for protein interaction studies. The procedures largely follow those of Haran and Ha (Boukobza *et al.*, 2001; Okumus *et al.*, 2004).

2.1. Lipid selection

The lipids for forming the membrane bilayer of the nanovesicles contain two components: one major lipid ($\sim 99\%$) that dominates the behavior of the membrane bilayer and the other minor lipid ($\sim 1\%$) that contains a biotin group for surface immobilization. The chemical nature and the gel-to-liquid phase transition temperature (T_m) of the major lipid are important here. The lipid must not significantly interact with the proteins and perturb the protein interactions. A lipid with a net zero charge is preferred, as it is less likely to interact with soluble, largely hydrophilic proteins (Boukobza *et al.*, 2001). Usually, the T_m of the major lipid should be much lower than the temperature for the single-molecule experiments, so the lipid bilayer stays in the fluidic liquid phase. A common major lipid used in single-molecule applications is Egg PC, extracted from egg yolk and $\sim 99\%$ of which is L- α -phosphatidylcholine. Its T_m is about -2°C (Silvius, 1983), so its bilayer is in the liquid phase at room temperature. Many other lipids with different T_m and charge properties are available and can be used for preparing vesicles (Silvius, 1983). For the biotinylated minor lipid, Biotinyl-cap PE (1,2-dipalmitoyl-*sn*-glycero-3-phosphoethanolamine-*N*-(cap biotinyl)) is commonly used.

2.2. Lipid nanovesicle preparation and protein trapping

The procedure consists of two major steps: (1) preparation of dry lipid film and hydration of the lipid film with buffer containing fluorescently labeled proteins to form vesicles and trap proteins inside and (2) extrusion of the formed vesicles through a polycarbonate membrane with well-defined pore diameters to make unilamellar vesicles of defined size. Using 100-nm pore-size membranes for extrusion, the multilamellar vesicles were estimated to be less than 2% (Hope *et al.*, 1985).

2.2.1. Lipid film preparation and hydration

1. Prepare lipid stock solutions in chloroform at 100 mg ml^{-1} and store them at $-20 \text{ }^\circ\text{C}$ in a desiccator. The biotinylated lipid stock solution is prepared at 1 mg ml^{-1} .
2. Transfer aliquots of lipid solutions into a clean glass test tube, forming a solution of $\sim 99\%$ major lipid and $\sim 1\%$ biotinylated minor lipid. Use enough amounts for a final total lipid concentration of 5 mg ml^{-1} upon hydration. Dry under a nitrogen flow until a thin lipid film is formed on the wall of the test tube. The lipid film can be further put under vacuum for 1–2 h to remove residual chloroform.
3. Hydrate the lipid film with the solution containing a mixture of the two labeled proteins under study. The concentration of each of the fluorescently labeled proteins should be close to the targeted effective concentration when the protein is trapped inside the nanovesicle. For example, for trapping a pair of protein molecules in 100 nm diameter nanovesicles, the concentration of each protein should be $\sim 3 \text{ } \mu\text{M}$, whereas for trapping in 200 nm diameter nanovesicles, use $\sim 400 \text{ nM}$ concentration. The efficiency of cotrapping a pair of molecules can be increased if the hydration and trapping are done under conditions where the protein pair has maximum binding affinity for each other.
4. Briefly vortex the hydrated solution to detach the lipid film from the wall of the test tube. Incubate the solution for 10 min to 1 h at a temperature of at least $10 \text{ }^\circ\text{C}$ above the T_m of the major lipid. The hydrated lipids will spontaneously form large multilamellar vesicles. Further freeze–thaw cycles (5–10 times) of the vesicle solution using liquid nitrogen and warm water can induce cracks in the membrane, which can improve entrapment of small molecules. Here, care must be taken that the freeze–thaw cycles do not denature the proteins; circular dichroism spectroscopy can be used to check the folding state of the protein.

2.2.2. Preparation of unilamellar nanovesicles via extrusion

Unilamellar nanovesicles are formed by extrusion of the vesicle solution through a polycarbonate membrane with nanometer-sized pores (Hope *et al.*, 1985; Johnson *et al.*, 2002; MacDonald *et al.*, 1991). Extrusion should

be performed at a temperature of at least 10 °C above the T_m of the major lipid. The Avanti mini extruder (Avanti Polar Lipids, Inc.) is handy for this purpose. Polycarbonate membranes of different pore diameters are available, ranging from 50 nm to 1 μ m. The nanovesicle diameter obtained after extrusion follows a Gaussian distribution, the width of which is dependent on the number of passes through the extruder; the more passes, the narrower the distribution (Hope *et al.*, 1985; MacDonald *et al.*, 1991). The diameter distribution can be checked using dynamic light scattering measurements. We normally perform tens of passes, significantly more than what is suggested by Avanti. The number of molecules trapped within the nanovesicles follows a Poisson distribution, the average occupation number depending on the protein/lipid ratio in the hydration step (Boukobza *et al.*, 2001). The exact occupancy of each nanovesicle can be determined by single-molecule fluorescence imaging (see Section 3.2).

3. SMFRET MEASUREMENTS OF WEAK PROTEIN-PROTEIN INTERACTIONS

The smFRET experiments consist of (1) immobilization of nanovesicles in a flow cell and (2) real-time imaging using total internal reflection fluorescence microscopy. The microscope is equipped with two-color detection for imaging the fluorescence of the FRET donor and acceptor simultaneously.

3.1. Surface immobilization of nanovesicles

To follow the protein-protein interactions inside each nanovesicle over time, the nanovesicles need to be immobilized on a surface. Most commonly, a biotin-avidin linkage is used. Biotinylated lipids in the nanovesicle membrane are used to bind avidins (e.g., streptavidin or neutravidin), which in turn are bound to a biotin-modified surface. We have used three different schemes to modify the surface with biotins, all of which yield similar results: (1) coating the surface with a lipid bilayer containing biotinylated lipids, (2) coating with biotinylated bovine serum albumin (BSA), and (3) coating with partially biotinylated polyethylene glycol (PEG).

3.1.1. Lipid bilayer coating

This surface modification scheme takes advantage of the spontaneous fusion of lipid vesicles onto clean quartz surfaces to form a lipid bilayer (Boxer, 2000; Brian and McConnell, 1984), over which the nanovesicles can be attached. The lipids used for this bilayer can be the same as those used for the nanovesicles, for example, 99% Egg PC and 1% Biotinyl-cap PE.

1. The procedure for lipid preparation is the same as described earlier. The lipid film is prepared first and then hydrated with buffer in the absence of proteins.
2. The hydrated solution is sonicated for 30 min to 1 h until clarity. The sonication here breaks large multilamellar vesicles to form small unilamellar vesicles, which can spontaneously fuse to clean quartz surfaces. The distribution of vesicle sizes is not important here.
3. Incubate the quartz substrate with the solution containing small unilamellar vesicles at a total lipid concentration of $1\text{--}5\text{ mg ml}^{-1}$ for 1 h. Wash out excess lipids from the quartz surface with buffer.
4. Vesicle preparation, surface coating, and washing should all be performed at a temperature of at least $10\text{ }^{\circ}\text{C}$ above the T_m of the major lipid.

One problem with using Egg PC for the supported bilayer is that at room temperature the bilayer exists in the liquid phase, so the attached nanovesicles are mobile. The nanovesicle mobility can be reduced by increasing the percentage of biotinylated lipid so that each nanovesicle is anchored to the supported bilayer by multiple biotin–avidin linkages (Okumus *et al.*, 2004). Nevertheless, many nanovesicles still remain mobile as we observed in our experiments. To alleviate this mobility problem, we have used another lipid, DPPC (1,2-dipalmitoyl-*sn*-glycero-3-phosphocholine), which has a T_m of $\sim 41\text{ }^{\circ}\text{C}$. Because of its high T_m , DPPC exists in the gel phase at room temperature, resulting in a mostly immobile lipid support.

3.1.2. BSA coating

BSA can bind to quartz surfaces strongly via nonspecific interactions (Rasnik *et al.*, 2005), and therefore, biotinylated BSA can be used to coat the quartz surface to immobilize nanovesicles:

1. Prepare 1 mg ml^{-1} biotinylated BSA solution and incubate on the quartz substrate for 30 min to 1 h.
2. Wash out excess biotin–BSA with buffer.

The BSA coating is easy to perform and can prevent rupture and fusion of nanovesicles to the quartz surface. (In case some bare patches on the glass surface exist because of incomplete coating with BSA, vesicle fusion to the glass surface can form patches of lipid bilayer to fill them up.)

3.1.3. PEG coating

Covalent functionalization of a quartz surface with partially biotinylated PEG is another scheme for immobilizing nanovesicles. The quartz surface is first covalently functionalized with amine groups, which are then covalently linked to PEG via succinimidyl ester chemistry.

- For amine modification:
 1. Prepare a fresh solution of 1.5–2% amino silane reagent (Vectabond, Vector Laboratories) in acetone. (Other types of amino silane reagents work too, for example, 3-aminopropyltriethoxysilane.)
 2. Drop 200 μl of the amino silane solution onto the quartz slide.
 3. Incubate for 5 min and then wash extensively with ultra-filtered, deionized water for 1 min. Dry the slides with nitrogen and store under a dry environment.
- For PEG modification:
 1. Prepare a solution of 98–99% m-PEG-SPA-5000 and 1–2% biotin-PEG-NHS-3400 (Nektar Therapeutics, JenKem Technology Inc., or SunBio, USA) in 100 mM NaHCO_3 , pH 8.2.
 2. Drop 200 μl of the PEG solution onto an amine-functionalized slide and sandwich it with another slide. Place parafilm spacers in between to prevent squeezing out the solution. Incubate for 4 h in the dark.
 3. Wash slides thoroughly with nanopure water and dry with nitrogen for usage.

3.2. Control experiments

3.2.1. Lipid–protein interactions

To check whether the fluorescently labeled proteins have nonspecific interactions with the lipid membrane, one can coat the quartz surface with a lipid bilayer and flow in solutions containing high concentrations (e.g., 100 nM) of labeled proteins. After washing the flow cell with fresh buffer and imaging the single-molecule fluorescence, the number of molecules that are immobilized on the lipid bilayer by nonspecific interactions can be counted. Comparing the number of nonspecifically bound molecules to the number of molecules detected using specific biotin–avidin immobilization of nanovesicles provides an estimate of the extent of nonspecific interactions between the protein and the lipid membrane (Benitez *et al.*, 2008, 2009; Okumus *et al.*, 2004).

3.2.2. Occupancy of nanovesicles

The nanovesicle trapping procedure will result in a distribution of occupancy of individual nanovesicles. The nanovesicle occupation is important to verify when using smFRET to study weakly interacting pairs. Under normal smFRET measurements, only the FRET donor is continuously excited and exhibits fluorescence. The FRET acceptor emits ideally only when it is close to the donor-labeled protein (e.g., upon protein–protein interaction) and is excited via energy transfer. The possible presence of multiple acceptor-labeled proteins within a nanovesicle can adversely affect quantitative determination of protein–protein interaction kinetics. Control

experiments are necessary to determine the distribution of occupancy of nanovesicles under the trapping conditions.

To do so, one can use two different lasers to excite the FRET donor and acceptor separately. For example, for the Cy3–Cy5 FRET pair, the Cy3 fluorescence can be directly imaged by excitation with a 532-nm laser and Cy5 fluorescence with a 637-nm laser. With the nanovesicles already loaded with fluorescent proteins and immobilized on the surface, the control experiments follow:

1. Directly excite the donor dye and record a movie of fluorescence intensity.
2. Switch to the second laser to excite the acceptor dye in the same area and record a fluorescence movie.
3. Analyze both movies to obtain fluorescence trajectories and positions of individual molecules. Use the number of photobleaching steps in the fluorescence intensity trajectory to determine the number of donor (or acceptor) molecules in the nanovesicle.
4. Check the position colocalization if the donor and acceptor dyes belong to the same nanovesicle. In our experience, incidental vesicle colocalization due to limited spatial resolution is minimal when the surface density of protein containing vesicles is smaller than $0.2 \mu\text{m}^{-2}$.

For weakly interacting protein pairs, such as Hah1 and MBD4 (see Section 3.3), the cotrapping efficiency is low. Among 340 nanovesicles containing either Hah1–Cy5 or MBD4–Cy3, only 21 of them contain a Hah1–Cy5 and a MBD4–Cy3.

The number of acceptor molecules can also be checked during normal smFRET measurements. One can first use the donor-exciting laser for smFRET while recording a fluorescence movie. In the later part of the movie, the acceptor-exciting laser is turned on to excite the acceptor dye until the acceptor photobleaches. The photobleaching events in the acceptor intensity will indicate the number of acceptor molecules in the nanovesicle. In this way, one is sure to examine only single pairs of protein molecules.

3.2.3. FRET differentiation of acceptor-blinked/bleached states from the dissociated state of protein interactions

Organic fluorescent dyes show blinking behavior, that is, the fluorescence intensity sometimes switches off temporarily. Although fluorescence blinking can be suppressed significantly by using an oxygen scavenging system and triplet quenchers (e.g., Trolox; Rasnik *et al.*, 2006), occasional blinking of the FRET acceptor is problematic, as it would result in an apparently low FRET efficiency ($E_{\text{FRET}} = I_A/(I_A + I_D)$, where I_A and I_D are the acceptor and donor fluorescence intensities), which could be mistaken as that of the dissociated state of protein–protein interactions. Fortunately, using nanovesicle trapping and Cy3–Cy5 as the FRET pair,

the Cy5-blinked state has clearly lower E_{FRET} than that of the dissociated state from control experiments (Benitez *et al.*, 2008, 2009).

As far as the apparent E_{FRET} is concerned, the acceptor-blinked state is effectively the same as that in the absence of the acceptor and that of the acceptor photobleached state. Therefore, the apparent E_{FRET} from nanovesicles that merely contain a donor molecule serves as a control for signal from the acceptor blinked state (Fig. 4.3A). The determined apparent E_{FRET} with one Cy3 only is 0.04 ± 0.05 , which is the same as Cy5-blinked/bleached state of a Cy3–Cy5 pair (Fig. 4.3C).

The dissociated state can be mimicked by a nanovesicle containing a free donor and a free acceptor (Fig. 4.3B), as the free dyes do not interact with each other. Here, the existence of both a donor and an acceptor must be confirmed by separate laser excitations (Fig. 4.3B). Under 532-nm excitation, the apparent E_{FRET} is 0.15 ± 0.14 (Fig. 4.3C); the larger value here compared with that of Cy5-blinked state is likely due to the residual direct excitation of Cy5 fluorescence by the 532-nm laser and some energy transfer of Cy3–Cy5 due to their confined coexistence inside the nanovesicle.

3.3. Application to weak interactions between intracellular copper transporters

We applied the nanovesicle trapping approach to enable smFRET studies of the weak, dynamic interactions between the human intracellular copper chaperone Hah1 and the fourth metal-binding domain (MBD4) of the copper transporting ATPase Wilson disease protein (WDP) (Benitez *et al.*, 2008, 2009). The interactions between Hah1 and WDP mediate the copper transfer from Hah1 to the MBDs of WDP, an essential process for safe trafficking of copper ions in human cells (Banci and Rosato, 2003; Cobine *et al.*, 2006; Huffman and O'Halloran, 2001; Kim *et al.*, 2008; Lutsenko *et al.*, 2007; Rosenzweig, 2001; Strausak *et al.*, 2003). Because of the low affinity of the Hah1–WDP interaction ($K_{\text{D}} \sim 10^{-6} \text{ M}$), their interaction dynamics have been challenging to quantify in ensemble measurements. Nanovesicle trapping offers an ideal platform to examine their interactions at the single-molecule level using smFRET.

We labeled Hah1 with the acceptor dye Cy5 and MBD4 with the donor dye Cy3, using maleimide chemistry at specific cysteine residues, and cotrapped them in 100-nm diameter nanovesicles. smFRET trajectories reveal their dynamic interactions (Fig. 4.4A). These trajectories show three different E_{FRET} states: E_0 (~ 0.2) is the dissociated state, and E_1 (~ 0.5) and E_2 (~ 0.9) are two different interaction complexes. Transitions between E_0 and E_1 and between E_0 and E_2 correspond to the binding/unbinding processes for forming complexes 1 and 2. The transitions between E_1 and E_2 correspond to the interconversions between the two

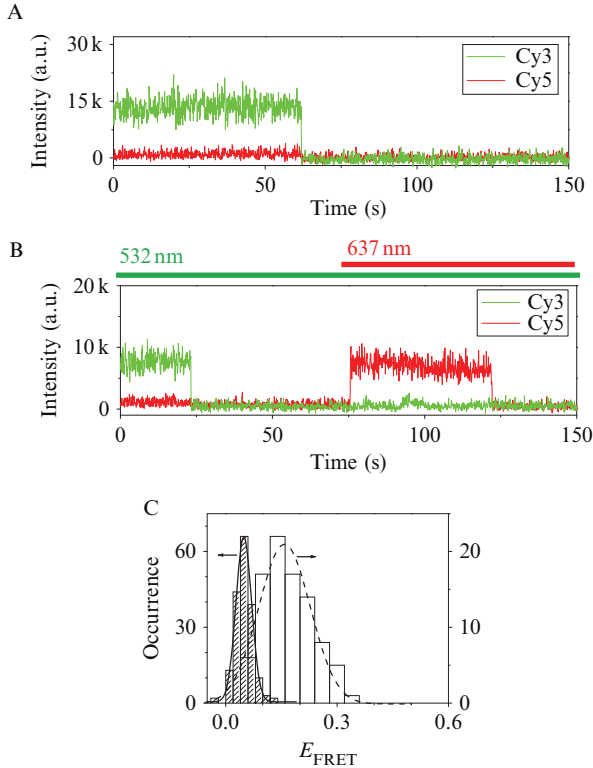


Figure 4.3 smFRET control experiments for acceptor blinked/bleached states and the dissociated state. (A) Two-color fluorescence intensity trajectories of a nanovesicle containing a single Cy3 molecule using 532-nm laser excitation. The Cy3 molecule photobleaches at the ~ 62 th second. (B) Two-color fluorescence intensity trajectories of a nanovesicle containing a single Cy3 and a single Cy5. The 532-nm laser is on throughout; the 637-nm laser was turned on at the ~ 75 th second. The Cy3 photobleaches at the ~ 25 th second; the Cy5 molecule photobleaches at ~ 125 th second. The first 25 seconds mimics the dissociated state of a Cy3–Cy5 pair. (C) Histograms of the apparent $E_{\text{FRET}} (=I_A/(I_A + I_D))$; I_D and I_A are the fluorescence intensities of the donor and acceptor, respectively) for nanovesicles containing a single Cy3 (line patterned columns) and for nanovesicles containing a free Cy3 and Cy5 molecule (clear columns).

complexes. Figure 4.4B gives the interaction scheme between Hah1 and MBD4. The kinetic constants of all interaction processes can be extracted by analyzing the distributions of dwell times in each FRET state (Fig. 4.4C–H, Section 4). The direct observation of the interconversion dynamics between the two interaction complexes is particularly exciting here, as it enables determination of both the forward and the reverse interconversion rate constants (see Section 4)—ensemble characterization can often only

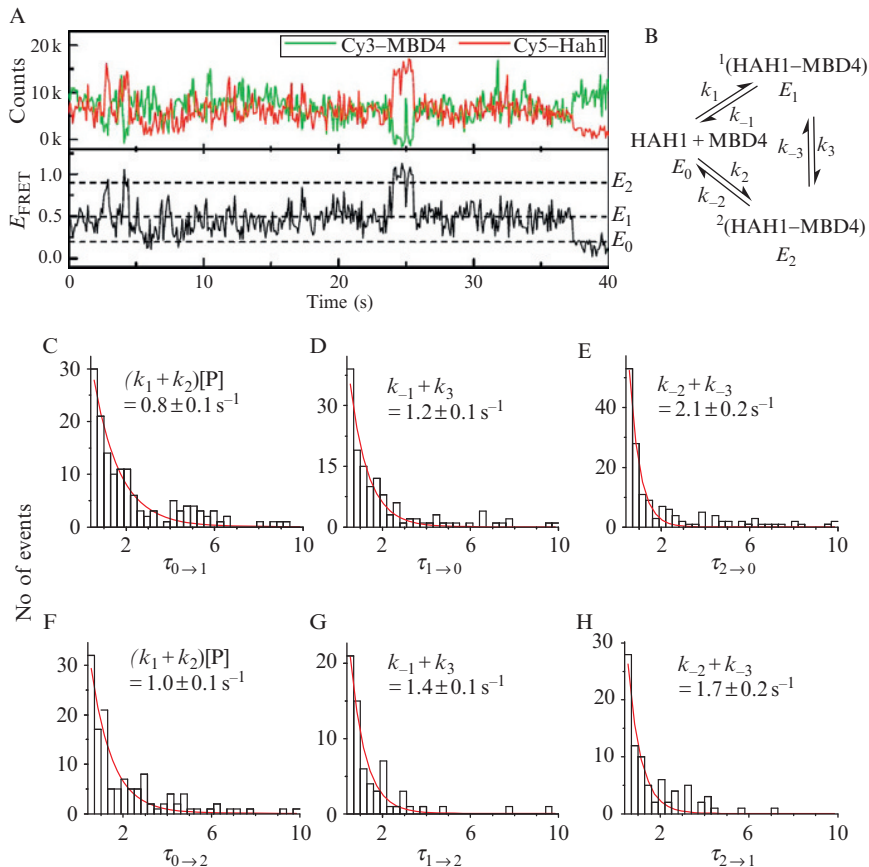


Figure 4.4 smFRET measurements of weak protein interaction dynamics in a nanovesicle. (A) Two-color fluorescence intensity (upper) and corresponding apparent E_{FRET} (lower) trajectories of a Cy5-Hah1 and a Cy3-MBD4 trapped in a 100-nm nanovesicle. (B) Interaction scheme between Hah1 and MBD4. (C–H) Distributions of the six types of dwell times from the E_{FRET} trajectories of Hah1-MBD4 interactions. Solid lines are exponential fits; insets give the exponential decay constants and their relations to the protein interaction rate constants in (B). [P] is the effective concentration ($\sim 3 \mu\text{M}$) of a single molecule in a 100-nm vesicle. The individual rate constants are $k_1 = (1.6 \pm 0.2) \times 10^5 \text{ M}^{-1} \text{ s}^{-1}$, $k_{-1} = 0.88 \pm 0.04 \text{ s}^{-1}$, $k_2 = (1.4 \pm 0.2) \times 10^5 \text{ M}^{-1} \text{ s}^{-1}$, $k_{-2} = 1.3 \pm 0.1 \text{ s}^{-1}$, $k_3 = 0.42 \pm 0.04 \text{ s}^{-1}$, and $k_{-3} = 0.7 \pm 0.1 \text{ s}^{-1}$. Data in (A, C–H) adapted with permission from Benitez *et al.* (2008, 2009). Copyright 2008 American Chemical Society. (See Color Insert).

determine the sum of the forward and reverse rates for intermediate interconversion dynamics, as the interconversion dynamics are generally nonsynchronizable.

4. SINGLE-MOLECULE KINETIC ANALYSIS OF THREE-STATE PROTEIN-PROTEIN INTERACTIONS

The interaction scheme between Hah1 and MBD4 can be generalized to that in Fig. 4.5A. An idealized E_{FRET} trajectory showing three FRET states is given in Fig. 4.5B with different types of dwell times denoted. In this section, we derive the probability density functions of the dwell times involved in this three-state interactions, using single-molecule kinetic analysis (Benitez *et al.*, 2008, 2009; Xie, 2001; Xu *et al.*, 2009).

We first consider the binding processes that occur during the dwell time τ_0 in the E_0 state. Based on the interaction scheme shown in Fig. 4.5A, the processes occurring during τ_0 are summarized in Scheme 4.1. The ensemble rate equations for these kinetic processes are

$$-\frac{d[A]}{dt} = -\frac{d[A']}{dt} = (k_1 + k_2)[A][A'] \quad (4.1a)$$

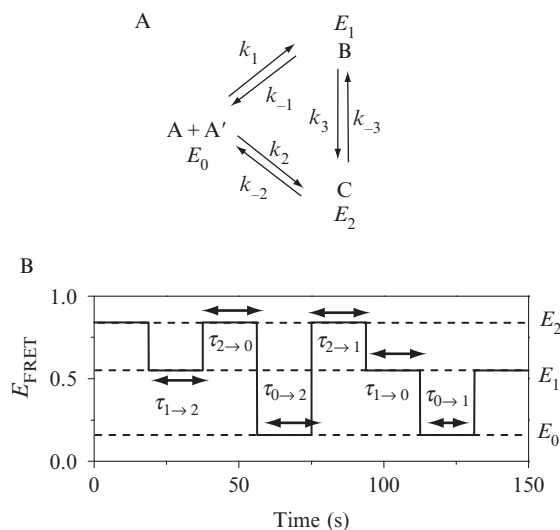
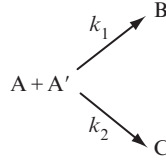


Figure 4.5 Generic kinetic scheme of protein interactions and corresponding E_{FRET} trajectories. (A) Generalized kinetic scheme of a single-interacting pair with three FRET states: one dissociated state, $A + A'$, with a FRET value of E_0 ; and two interaction complexes, B and C, with FRET values of E_1 and E_2 , respectively. (B) Idealized three-state E_{FRET} trajectories of an interacting pair; all six types of dwell times are denoted.



Scheme 4.1 Kinetic processes occurring during the dwell time τ_0 at the E_0 state.

$$\frac{d[\text{B}]}{dt} = k_1[\text{A}][\text{A}'] \quad (4.1b)$$

$$\frac{d[\text{C}]}{dt} = k_2[\text{A}][\text{A}'] \quad (4.1c)$$

For the single-molecule reactions occurring in a nanovesicle, we have to consider the molecules in terms of their probabilities at time t , $P(t)$. These rate equations then become

$$-\frac{dP_{\text{A}}(t)}{dt} = -\frac{dP_{\text{A}'}(t)}{dt} = (k_1 + k_2)P_{\text{A}}(t)P_{\nu, \text{A}', \text{A}}(t) \quad (4.2a)$$

$$\frac{dP_{\text{B}}(t)}{dt} = k_1P_{\text{A}}(t)P_{\nu, \text{A}', \text{A}}(t) \quad (4.2b)$$

$$\frac{dP_{\text{C}}(t)}{dt} = k_2P_{\text{A}}(t)P_{\nu, \text{A}', \text{A}}(t) \quad (4.2c)$$

Here $P_{\text{A}}(t)$ is the probability of finding A at time t ; $P_{\text{A}'}(t)$, $P_{\text{B}}(t)$, and $P_{\text{C}}(t)$ are defined similarly; and $P_{\text{A}}(t) + P_{\text{B}}(t) + P_{\text{C}}(t) = 1$. $P_{\nu, \text{A}', \text{A}}(t)$ is the *conditional* probability at time t of finding A' within the same infinitesimal volume ν where A is located, provided that A is found. $P_{\nu, \text{A}', \text{A}}(t)$ is then

$$P_{\nu, \text{A}', \text{A}}(t) = \frac{P_{\text{A}', \text{A}}(t)}{V} \quad (4.3)$$

Here $P_{\text{A}', \text{A}}(t)$ is the *conditional* probability at time t of finding A' within the entire space of the nanovesicle, provided that A is found; and V is the volume of the nanovesicle. Because whenever A is present, A' is found, $P_{\text{A}', \text{A}}(t) = 1$. Therefore, $P_{\nu, \text{A}', \text{A}}(t) = 1/V$, which is the effective concentration (c_{eff}) of one molecule inside the nanovesicle. We then have

$$-\frac{dP_{\text{A}}(t)}{dt} = -\frac{dP_{\text{A}'}(t)}{dt} = (k_1 + k_2)c_{\text{eff}}P_{\text{A}}(t) \quad (4.4a)$$

$$\frac{dP_B(t)}{dt} = k_1 c_{\text{eff}} P_A(t) \quad (4.4b)$$

$$\frac{dP_C(t)}{dt} = k_2 c_{\text{eff}} P_A(t) \quad (4.4c)$$

The initial conditions for solving these equations are $P_A(0) = P_{A'}(0) = 1$, $P_B(0) = 0$, and $P_C(0) = 0$, with $t = 0$ being the onset of each binding reaction.

We can then evaluate the probability density $f_0(\tau)$ of the dwell time τ_0 . The probability of finding a particular τ_0 is $f_0(\tau)\Delta\tau$; and $f_0(\tau)\Delta\tau$ is equal to the sum of two probabilities: (1) the probability of molecule A and A' to form B between $t = \tau$ and $\tau + \Delta\tau$, which is $\Delta P_B(\tau) = k_1 c_{\text{eff}} P_A(\tau)\Delta\tau$; and (2) the probability of molecule A and A' to form C between $t = \tau$ and $\tau + \Delta\tau$, which is $\Delta P_C(\tau) = k_2 c_{\text{eff}} P_A(\tau)\Delta\tau$. In the limit of infinitesimal $\Delta\tau$,

$$f_0(\tau) = \frac{d(P_B(\tau) + P_C(\tau))}{d\tau} = (k_1 + k_2) c_{\text{eff}} P_A(\tau) \quad (4.5)$$

Using the initial conditions to solve Eqs. (4.4a)–(4.4c) for $P_A(\tau)$, we get

$$f_0(\tau) = (k_1 + k_2) c_{\text{eff}} \exp[-(k_1 + k_2) c_{\text{eff}} \tau] \quad (4.6a)$$

Clearly, $\int_0^\infty f_0(\tau) d\tau = 1$, as expected.

The dwell time τ_0 can be further separated into two types: one, $\tau_{0 \rightarrow 1}$, that ends with a transition to the E_1 state and the other, $\tau_{0 \rightarrow 2}$, that ends with a transition to the E_2 state. We can also evaluate the corresponding probability densities $f_{0 \rightarrow 1}(\tau)$ and $f_{0 \rightarrow 2}(\tau)$ of the dwell times $\tau_{0 \rightarrow 1}$ and $\tau_{0 \rightarrow 2}$. The probability of finding a particular $\tau_{0 \rightarrow 1}$ is $f_{0 \rightarrow 1}(\tau)\Delta\tau$; and $f_{0 \rightarrow 1}(\tau)\Delta\tau$ is equal to the probability for A and A' to form B between $t = \tau$ and $\tau + \Delta\tau$, which is $\Delta P_B(\tau) = k_1 c_{\text{eff}} P_A(\tau)\Delta\tau$. The probability of finding a particular $\tau_{0 \rightarrow 2}$ is $f_{0 \rightarrow 2}(\tau)\Delta\tau$; and $f_{0 \rightarrow 2}(\tau)\Delta\tau$ is equal to the probability for A and A' to form C between $t = \tau$ and $\tau + \Delta\tau$, which is $\Delta P_C(\tau) = k_2 c_{\text{eff}} P_A(\tau)\Delta\tau$. In the limit of infinitesimal $\Delta\tau$:

$$f_{0 \rightarrow 1}(\tau) = \frac{dP_B(\tau)}{d\tau} = k_1 c_{\text{eff}} \exp[-(k_1 + k_2) c_{\text{eff}} \tau] \quad (4.6b)$$

$$f_{0 \rightarrow 2}(\tau) = \frac{dP_C(\tau)}{d\tau} = k_2 c_{\text{eff}} \exp[-(k_1 + k_2) c_{\text{eff}} \tau] \quad (4.6c)$$

Expectedly, $f_{0 \rightarrow 1}(\tau) + f_{0 \rightarrow 2}(\tau) = f_0(\tau)$. Note the exponential decay constants of $f_{0 \rightarrow 1}(\tau)$ and $f_{0 \rightarrow 2}(\tau)$ are the same as that of $f_0(\tau)$, all equal to $(k_1 + k_2) c_{\text{eff}}$, the sum of the two parallel kinetic processes in Scheme 4.1. The ratio between the total occurrence $N_{0 \rightarrow 1}$ of dwell time $\tau_{0 \rightarrow 1}$ and the total

occurrence $N_{0 \rightarrow 2}$ of dwell time $\tau_{0 \rightarrow 2}$ in the smFRET trajectories also carries important information:

$$\frac{N_{0 \rightarrow 1}}{N_{0 \rightarrow 2}} = \frac{\int_0^\infty f_{0 \rightarrow 1}(\tau) d\tau}{\int_0^\infty f_{0 \rightarrow 2}(\tau) d\tau} = \frac{k_1}{k_2} \quad (4.6d)$$

Similarly, we can derive the probability density function of the dwell time τ_1 on the E_1 state, which can be separated into two types: $\tau_{1 \rightarrow 0}$ and $\tau_{1 \rightarrow 2}$, and that of the dwell time τ_2 on the E_2 state, which can be separated into $\tau_{2 \rightarrow 0}$ and $\tau_{2 \rightarrow 1}$. The results are

$$f_1(\tau) = (k_{-1} + k_3) \exp[-(k_{-1} + k_3)\tau] \quad (4.7a)$$

$$f_{1 \rightarrow 0}(\tau) = k_{-1} \exp[-(k_{-1} + k_3)\tau] \quad (4.7b)$$

$$f_{1 \rightarrow 2}(\tau) = k_3 \exp[-(k_{-1} + k_3)\tau] \quad (4.7c)$$

$$\frac{N_{1 \rightarrow 0}}{N_{1 \rightarrow 2}} = \frac{k_{-1}}{k_3} \quad (4.7d)$$

$$f_2(\tau) = (k_{-2} + k_{-3}) \exp[-(k_{-2} + k_{-3})\tau] \quad (4.8a)$$

$$f_{2 \rightarrow 0}(\tau) = k_{-2} \exp[-(k_{-2} + k_{-3})\tau] \quad (4.8b)$$

$$f_{2 \rightarrow 1}(\tau) = k_{-3} \exp[-(k_{-2} + k_{-3})\tau] \quad (4.8c)$$

$$\frac{N_{2 \rightarrow 0}}{N_{2 \rightarrow 1}} = \frac{k_{-2}}{k_{-3}} \quad (4.8d)$$

Equations (4.6a)–(4.6d), (4.7a)–(4.7d), and (4.8a)–(4.8d) can be used to fit the corresponding experimental results to obtain the rate constants. The caption of Fig. 4.4C gives the determined rate constants for each of the kinetic steps in the Hah1–MBD4 interaction, from which the K_D 's of the interaction complexes can be calculated. In ensemble-averaged measurements, if the two interaction complexes cannot be differentiated but are detectable, the measured effective dissociation constant ($K_{D,\text{eff}}$) is related to the K_D 's of the two complexes as $1/K_{D,\text{eff}} = 1/K_{D1} + 1/K_{D2}$.

5. FURTHER DEVELOPMENTS

A limitation of using Egg PC for forming nanovesicles is the enclosed environment that prevents facile exchange of solution. Being able to change the solution condition and introduce additional chemical reagents is highly

desired, however. Ha and coworkers have developed two strategies to make the nanovesicles porous to allow exchange of solution into the nanovesicles (Cisse *et al.*, 2007): (1) using a lipid with a higher T_m and performing experiments at its T_m , which induces defects in the lipid membrane and (2) incorporating into the bilayer membrane the bacterial toxin α -hemolysin that forms pores.

The first strategy is based on the fact that lipid bilayer membranes form packing defects at T_m , making the membrane permeable to small molecules (Chakrabarti and Deamer, 1992; Monnard, 2003). Ha and coworkers used the lipid DMPC (1,2-dimyristoyl-*sn*-glycero-3-phosphocholine), which has a T_m of ~ 23 °C. They showed that at ~ 23 °C, the nanovesicles made of DMPC lipid membranes are permeable to molecules as large as ATP, but not to macromolecules such as proteins and DNA. The second strategy uses the natural pore-forming ability of the membrane protein α -hemolysin, a heptameric transmembrane channel from *Staphylococcus aureus*. The monomers of α -hemolysin self-assemble into the heptameric channel structure in a lipid bilayer, forming a stable pore of 1.4–2.4 nm diameter and allowing exchange of most solution components (Song *et al.*, 1996).

The lipid membrane of the nanovesicles also provides a natural platform for studying protein interactions that involve membrane-bound or membrane-anchored proteins. To do so, one can incorporate or anchor one protein to the lipid membrane of the nanovesicle and trap the other protein inside. smFRET measurements can then be employed to monitor their interactions at high effective concentrations.

The confined volume of the nanovesicles can also be exploited to probe the crowding effects on protein interactions by cotrapping a larger number of different types of unlabeled macromolecules inside, for example polysaccharides. This crowding effect arguably mimics the intracellular environment, offering an opportunity to study biomacromolecule dynamics in a controlled and confined environment *in vitro*.

6. CONCLUDING REMARKS

Nanovesicle trapping is a convenient approach to enabling single-molecule studies at high effective concentrations. This approach also offers easy surface immobilization and minimization of nonspecific interactions with glass surfaces. Coupled with smFRET measurements, dynamic events of protein interactions with weak affinity can be monitored in real time at the single-molecule level. Single-molecule kinetic analysis allows extraction of quantitative kinetics of the protein interactions, some of which are challenging to quantify with ensemble techniques. The lipid membrane also mimics the cellular environment, as well as provides a natural platform

for studying membrane-bound or membrane-anchored proteins. The confined volume can further be exploited to study crowding effects on macromolecule dynamics at the single-molecule level. With porous vesicles allowing solution exchange, many biological processes can be studied at high effective concentrations *in situ*. We expect that more biological studies using the nanovesicle trapping approach will emerge.

ACKNOWLEDGMENTS

This research is supported by the National Science Foundation (CHE0645392), National Institute of Health (GM082939), the Wilson Disease Association, a Camille and Henry Dreyfus New Faculty Award, an Alfred P. Sloan Fellowship, and Cornell University. J. J. B. and A. M. K. are supported by Molecular Biophysics Traineeships from the National Institute of Health. We thank Prof. D. L. Huffman and A. R. Rosenzweig for their collaboration.

REFERENCES

- Banci, L., and Rosato, A. (2003). Structural genomics of proteins involved in copper homeostasis. *Acc. Chem. Res.* **36**, 215–221.
- Benitez, J. J., Keller, A. M., Ochieng, P., Yatsunyk, L. A., Huffman, D. L., Rosenzweig, A. C., and Chen, P. (2008). Probing real-time transient metallochaperone–target protein interactions at the single-molecule level with nanovesicle trapping. *J. Am. Chem. Soc.* **130**, 2446–2447.
- Benitez, J. J., Keller, A. M., Ochieng, P., Yatsunyk, L. A., Huffman, D. L., Rosenzweig, A. C., and Chen, P. (2009). Correction/addition: Probing real-time transient metallochaperone–target protein interactions at the single-molecule level with nanovesicle trapping. *J. Am. Chem. Soc.* **131**, 871.
- Boukobza, E., Sonnenfeld, A., and Haran, G. (2001). Immobilization in surface-tethered lipid vesicles as a new tool for single biomolecule spectroscopy. *J. Phys. Chem. B*, **105**, 12165–12170.
- Boxer, S. G. (2000). Molecular transport and organization in supported lipid membranes. *Curr. Opin. Cell Biol.* **4**, 704–709.
- Brian, A. A., and McConnell, H. M. (1984). Allogeneic stimulation of cytotoxic T cells by supported planar membranes. *Proc. Natl. Acad. Sci. USA* **81**, 6159–6163.
- Chakrabarti, A. C., and Deamer, D. W. (1992). Permeability of lipid bilayers to amino acids and phosphate. *Biochim. Biophys. Acta* **1111**, 171–177.
- Chiu, D. T., Wilson, C. F., Karlsson, A., Danielsson, A., Lundqvist, A., Strömberg, A., Ryttsén, F., Davidson, M., Nordholm, S., Orwar, O., and Zare, R. N. (1999). Manipulating the biochemical nanoenvironment around single molecules contained within vesicles. *Chem. Phys.* **247**, 133–139.
- Cisse, I., Okumus, B., Joo, C., and Ha, T. (2007). Fueling protein–DNA interactions inside porous nanocontainers. *Proc. Natl. Acad. Sci. USA* **104**, 12646–12650.
- Cobine, P. A., Pierrel, F., and Winge, D. R. (2006). Copper trafficking to the mitochondrion and assembly of copper metalloenzymes. *Biochim. Biophys. Acta* **1763**, 759–772.
- Gragеров, A., Nudler, E., Komissarova, N., Gaitanaris, G. A., Gottesman, M. E., and Nikiforov, V. (1992). Cooperation of GroEL/GroES and DnaK/DnaJ heat shock proteins in preventing protein misfolding in *Escherichia coli*. *Proc. Natl. Acad. Sci. USA* **89**, 10341–10344.

- Hall, A. (1992). Ras-related GTPases and the cytoskeleton. *Mol. Biol. Cell* **3**, 475–479.
- Haran, G. (2003). Single-molecule fluorescence spectroscopy of biomolecular folding. *J. Phys. Condens. Matter* **15**, R1291–R1317.
- Hope, M. J., Bally, M. B., Webb, G., and Cullis, P. R. (1985). Production of large unilamellar vesicles by a rapid extrusion procedure. Characterization of size distribution, trapped volume and ability to maintain a membrane potential. *Biochim. Biophys. Acta* **812**, 55–65.
- Huffman, D. L., and O'Halloran, T. V. (2001). Function, structure, and mechanism of intracellular copper trafficking proteins. *Annu. Rev. Biochem.* **70**, 677–701.
- Johnson, J. M., Ha, T., Chu, S., and Boxer, S. G. (2002). Early steps of supported bilayer formation probed by single vesicle fluorescence assays. *Biophys. J.* **83**, 3371–3379.
- Kim, B.-E., Nevitt, T., and Thiele, D. J. (2008). Mechanisms for copper acquisition, distribution and regulation. *Nat. Chem. Biol.* **4**, 176–185.
- Laurence, T. A., and Weiss, S. (2003). How to detect weak pairs. *Science* **299**, 667–668.
- Lee, J. Y., Okumus, B., Kim, D. S., and Ha, T. (2005). Extreme conformational diversity in human telomeric DNA. *Proc. Natl. Acad. Sci. USA* **102**, 18938–18943.
- Levene, M. J., Korch, J., Turner, S. W., Foquet, M., Craighead, H. G., and Webb, W. W. (2003). Zero-mode waveguide for single-molecule analysis at high concentration. *Science* **299**, 682–686.
- Lutsenko, S., LeShane, E. S., and Shinde, U. (2007). Biochemical basis of regulation of human copper-transporting ATPase. *Arch. Biochem. Biophys.* **463**, 134–148.
- MacDonald, R. C., MacDonald, R. I., Menco, B. E., Takeshita, K., Subbarao, N. K., and Hu, L. R. (1991). Small-volume extrusion apparatus for preparation of large, unilamellar vesicles. *Biochim. Biophys. Acta* **1061**, 297–303.
- Monnard, P.-A. (2003). Liposome-entrapped polymerases as models for microscale/nanoscale bioreactors. *J. Membr. Biol.* **191**, 87–97.
- Nooren, I. M. A., and Thornton, J. M. (2003). Diversity of protein–protein interactions. *EMBO J.* **22**, 3486–3492.
- Okumus, B., Wilson, T. J., Lilley, D. M. J., and Ha, T. (2004). Vesicle encapsulation studies reveal that single molecule ribozyme heterogeneities are intrinsic. *Biophys. J.* **87**, 2798–2806.
- Rasnik, I., McKinney, S. A., and Ha, T. (2005). Surfaces and orientations: Much to FRET about? *Acc. Chem. Res.* **38**, 542–548.
- Rasnik, I., McKinney, S. A., and Ha, T. (2006). Nonblinking and long-lasting single molecule fluorescence imaging. *Nat. Methods* **3**, 891–893.
- Rhoades, E., Gussakovsky, E., and Haran, G. (2003). Watching proteins fold one molecule at a time. *Proc. Natl. Acad. Sci. USA* **100**, 3197–3202.
- Rhoades, E., Cohen, M., Schuler, B., and Haran, G. (2004). Two-state folding observed in individual protein molecules. *J. Am. Chem. Soc.* **126**, 14686–14687.
- Rosenzweig, A. C. (2001). Copper delivery by metallochaperone proteins. *Acc. Chem. Res.* **34**, 119–128.
- Silvius, J. R. (1983). Thermotropic phase transitions of pure lipids in model membranes and their modifications by membrane proteins. In “Lipid–Protein Interactions,” (P. C. Jost and O. H. Griffiths, eds.), pp. 239–281. Wiley, New York.
- Song, L., Hobaugh, M. R., Shustak, C., Cheley, S., Bayley, H., and Gouaux, J. E. (1996). Structure of staphylococcal-hemolysin a heptameric transmembrane pore. *Science* **274**, 1859–1865.
- Strausak, D., Howies, M. K., Firth, S. D., Schlicksupp, A., Pipkorn, R., Multhaupt, G., and Mercer, J. F. B. (2003). Kinetic analysis of the interaction of the copper chaperone Atox1 with the metal binding sites of the menkes protein. *J. Biol. Chem.* **278**, 20821–20827.
- Xie, X. S. (2001). Single-molecule approach to enzymology. *Single Mol.* **2**, 229–236.
- Xu, W., Kong, J. S., and Chen, P. (2009). Single-molecule kinetic theory of heterogeneous and enzyme catalysis. *J. Phys. Chem. C* **113**, 2393–2404.